ACS Catalysis

Research Article

pubs.acs.org/acscatalysis

Theoretical Analysis of Cobalt Hangman Porphyrins: Ligand Dearomatization and Mechanistic Implications for Hydrogen Evolution

Brian H. Solis,[†] Andrew G. Maher,[‡] Tatsuhiko Honda,[‡] David C. Powers,[‡] Daniel G. Nocera,[‡] and Sharon Hammes-Schiffer*[,†]

[†]Department of Chemistry, University of Illinois at Urbana-Champaign, 600 South Mathews Avenue, Urbana, Illinois 61801, United States

[‡]Department of Chemistry and Chemical Biology, Harvard University, 12 Oxford Street, Cambridge, Massachusetts 02138-2902, United States

Supporting Information

ABSTRACT: The design of molecular electrocatalysts for hydrogen evolution has been targeted as a strategy for the conversion of solar energy to chemical fuels. In cobalt hangman porphyrins, a carboxylic acid group on a xanthene backbone is positioned over a metalloporphyrin to serve as a proton relay. A key proton-coupled electron transfer (PCET) step along the hydrogen evolution pathway occurs via a sequential ET-PT mechanism in which electron transfer (ET) is followed by proton transfer (PT). Herein theoretical calculations are employed to investigate the mechanistic pathways of these hangman metalloporphyrins. The calculations confirm the ET-PT mechanism by illustrating that the calculated reduction potentials for this mechanism are consistent with experimental data. Under strong-acid conditions, the calculations indicate that this catalyst evolves H_2 by protonation of a formally Co(II) hydride intermediate, as suggested by previous experiments. Under weak-acid conditions, however, the calculations reveal a mechanism that proceeds via a phlorin intermediate, in which the *meso* carbon of the porphyrin is protonated. In the first electrochemical reduction, the neutral Co(II) species is reduced to a monoanionic singlet Co(I) species. Subsequent reduction leads to a dianionic doublet, formally a Co(0) complex in which substantial mixing of Co and porphyrin orbitals indicates ligand redox noninnocence. The partial reduction of the ligand disrupts the aromaticity in the porphyrin ring. As a result of this ligand dearomatization, protonation of the dianionic species is significantly more thermodynamically favorable at the *meso* carbon than at the metal center, and the ET-PT mechanism leads to a dianionic phlorin species. According to the proposed mechanism, the carboxylate group of this dianionic phlorin species is reprotonated, the species is reduced again, and H_2 is evolved from the protonated carboxylate and the protonated carbon. This proposed mechanism is a guidepost for future experimental studies of proton relays involving noninnocent ligand platforms.

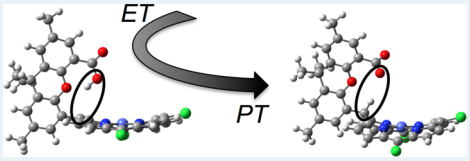

KEYWORDS: *proton-coupled electron transfer, hydrogen evolution reaction, hangman porphyrin, electrocatalyst, proton relay, dearomatization, phlorin*

INTRODUCTION

Efficient conversion of solar energy into chemical bonds is important for global sustainability.[1] The hydrogen evolution reaction (HER), oxidation of water to oxygen, and reduction of CO_2 to hydrocarbons are multielectron, multiproton processes.[2] In these reactions, electron transfer (ET) and proton transfer (PT) steps often occur as proton-coupled electron transfer (PCET) reactions.[3−9] PCET can occur sequentially, with the initial ET or PT forming a stable intermediate, or concertedly, with ET and PT occurring simultaneously. Incorporating proton relays into molecular electrocatalysts facilitates PCET by juxtaposing the proton donor and acceptor.[10−16] A fundamental understanding of PCET through molecular proton relays can assist in the design of efficient HER electrocatalysts.[17−23]

A series of metalloporphyrins has been studied as HER electrocatalysts in acetonitrile.[24,25] In the case of the cobalt "hangman" porphyrin ([**1**-H], Chart 1), in which a carboxylic acid group affixed to a xanthene backbone is positioned over a metalloporphyrin capable of electrochemical reduction, a PCET step along the HER pathway was shown to occur by a sequential ET-PT mechanism. Specifically, the formal Co(I) state was proposed to be reduced to Co(0) and then quickly protonated intramolecularly from the hangman moiety to form a Co(II) hydride intermediate. Electrokinetic studies revealed the intramolecular PT rate constant to be ca. 8.5×10^6 s^{-1}.[25] The non-hangman analogue [**2**] (Chart 1) behaves similarly to [**1**-H] electrochemically but evolves hydrogen at a more negative potential (E_{cat}[**1**] ≈ −1.9 V vs Fc^+/Fc; E_{cat}[**2**] ≈ −2.1 V vs Fc^+/Fc) with benzoic acid due to the lack of an internal proton relay.[24]

Received: September 24, 2014
Revised: November 3, 2014
Published: November 6, 2014

   dx.doi.org/10.1021/cs501454y | ACS Catal. 2014, 4, 4516−4526

Chart 1. Structure of Cobalt Porphyrins

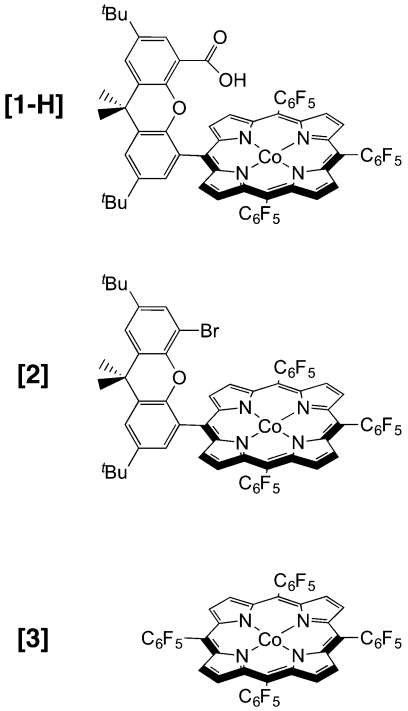

In this work, we employ computational methods to investigate potential mechanisms of hydrogen evolution catalyzed by cobalt metalloporphyrins. NMR experiments were performed to probe the spin state of $[\mathbf{3}]^-$ (Chart 1) to assist in the selection of a suitable level of theory. We investigate several intramolecular PT pathways by allowing the proton to transfer from the hangman moiety of [**1-H**] to the cobalt center, a pyrrolic nitrogen, or the closest *meso* carbon. Calculated relative pK_as are used to explore additional intermolecular PT steps preceding H_2 production. Reduction potentials are calculated for the ET steps in the ET-PT, PT-ET, and concerted PCET mechanisms for all proton acceptors. Additionally, we calculate a transition state structure for the PT reaction within the experimentally proposed ET-PT mechanism and employ transition state theory to calculate a first-order PT rate constant to compare to previous experimental results. On the basis of the calculations, we propose mechanisms for the HER catalyzed by Co hangman porphyrins in both weak- and strong-acid regimes.

COMPUTATIONAL METHODS

The complexes were optimized with density functional theory (DFT), primarily with the BP86 functional.[26,27] Additional benchmarking was performed with the following functionals and is presented in the Supporting Information: B3P86,[26,28] B3LYP,[28,29] BLYP,[27,29] TPSSh,[30] M06L,[31] and ωB97XD.[32−35] Geometry optimizations were performed with the 6-31+G(d,p)[36] basis set for the transferring proton and the 6-31+G(d)[37−39] basis set for all remaining atoms with default options in Gaussian 09.[40] The results presented in the main paper are based on the structures optimized in solution; structures optimized in the gas phase are provided in the Supporting Information and are similar to those optimized in solution. Calculations in acetonitrile solvent utilized the conductor-like polarizable continuum model (C-PCM)[41,42] with Bondi radii and included nonelectrostatic interactions resulting from dispersion,[43,44] repulsion,[44] and cavity formation.[45] Entropic and zero-point energy effects from the vibrational frequencies at T = 298.15 K were included in the calculation of the reaction free energies. The free energies of the solvated molecules calculated with geometries optimized in the gas phase, which are presented in the Supporting Information, employed a Born−Haber thermodynamic cycle that combined gas-phase free energies with single-point solvation free energies of the reactant and product species.[46,47] For computational tractability, the pentafluorophenyl groups were replaced with chlorines and the *tert*-butyl groups were replaced with methyl groups. These substitutions were chosen on the basis of similar electron-donating or electron-withdrawing properties as determined by their Hammett constants (Table S1, Supporting Information).[48,49]

Reduction potentials were calculated using the relation $\Delta G^\circ_{redox} = -nFE^\circ$, where n is the number of transferring electrons, F is Faraday's constant, and ΔG°_{redox} is the free energy of reduction. The free energies of reduction were calculated using the expression $\Delta G^\circ_{redox} = \Delta H^\circ - T\Delta S^\circ$ for structures optimized in solution. Reference reactions were utilized in the calculation of reduction potentials to eliminate systematic errors in DFT, limitations in the basis sets and exchange-correlation functionals, and changes in standard states.[46,47] All reduction potentials were calculated with respect to the ferrocenium/ferrocene couple (Fc^+/Fc) in acetonitrile. Axial solvent ligands may bind to an open octahedral site of cobalt d^7 complexes, consistent with the crystal structure of a related Co(II) hangman porphyrin that contains an axial ligand.[50] Given the excellent agreement of the calculated Co(II/I) and Co(I/0) reduction potentials with experiment, however, no axial solvent ligands were explicitly included in the calculations. In some cases, an explicit water molecule was included to test the effects of residual water on possible intramolecular proton transfer mechanisms.

The pK_a calculations were performed using the relation $\Delta G^\circ_{pK_a} = [\ln(10)RT]pK_a$, where $\Delta G^\circ_{pK_a}$ is the free energy of deprotonation. The free energies of deprotonation were calculated using the expression $\Delta G^\circ_{pK_a} = \Delta H^\circ - T\Delta S^\circ$ for structures optimized in solution. Relative pK_as were calculated with experimentally known references: the deprotonation of $[\mathbf{1}\text{-}\mathbf{H}]^0$ (determined to be 20.2 in acetonitrile)[51] and the deprotonation of the Co hydride $[\mathbf{3}\text{-}\mathbf{H}_{Co}]^0$ (estimated to be 15.0). This latter estimate stems from the rise in a catalytic wave of [**1-H**] and [**2**] at ca. −1.5 V vs Fc^+/Fc with *p*-toluenesulfonic (tosic) acid (pK_a = 8.0)[52] but not benzoic acid (pK_a = 20.7),[53] providing a range of plausible Co(III) hydride pK_a values.[24] The choice of pK_a = 15.0 for $[\mathbf{3}\text{-}\mathbf{H}_{Co}]^0$ is validated by calculations of relative pK_as that fall in the appropriate range. As with reduction potentials, systematic errors in DFT cancel in the calculation of relative pK_as.[47] Two pK_a references are needed in the calculations to obtain reasonable pK_a values of singly and multiply protonated complexes. All calculations that result in the deprotonated $[\mathbf{1}]^-$, $[\mathbf{1}]^{2-}$, or $[\mathbf{1}]^{3-}$ are calculated with respect to the $[\mathbf{1}\text{-}\mathbf{H}]^0$ pK_a reference, while all other calculated relative pK_as are calculated with respect to the $[\mathbf{3}\text{-}\mathbf{H}_{Co}]^0$ pK_a reference.

A transition state for PT was calculated with the synchronous transit-guided quasi-Newton method.[54,55] The reactant and product states were aligned in Cartesian space and interpolated to obtain the average structure, which was used as a guess for the transition state geometry. The transition state structure was

dx.doi.org/10.1021/cs501454y | ACS Catal. 2014, 4, 4516−4526

confirmed to contain a single imaginary frequency corresponding to the PT mode. The intrinsic reaction coordinate was followed backward and forward to the expected reactant and product species. The free energy barrier for PT was used in conjunction with transition state theory to calculate the PT rate constant:

$$k_{PT} = \frac{k_B T}{h} \exp\left(\frac{-\Delta G^{\ddagger}}{k_B T}\right) \quad (1)$$

where k_B is Boltzmann's constant, T is the temperature, h is Planck's constant, and $\Delta G^{\ddagger}$ is the free energy barrier. Here we are neglecting the effects of dynamical barrier recrossings and tunneling.

RESULTS AND DISCUSSION

Electronic Structure and H_2 Evolution Mechanism of [3]. Analyses of the spin densities and molecular orbitals of [3] provide insight into the electronic structure of the cobalt porphyrins along the hydrogen evolution reaction pathway. The low-spin Co(II) complex $[3]^0$ is reduced to singlet Co(I) $[3]^-$, the spin state of which was determined by ^{1}H NMR (Figure S1, Supporting Information) and is consistent with literature reports for other one-electron-reduced Co porphyrins.[56,57] The formally Co(0) structure $[3]^{2-}$ was calculated to be a doublet with spin density on the cobalt approximately 0.5, suggesting substantial metal−ligand orbital mixing with partial reduction of the ligand. On the basis of the computed spin density, we describe the formally Co(0) structure as Co("0.5"). The highest occupied molecular orbitals (HOMOs) of $[3]^-$ and $[3]^{2-}$ are depicted in Figure 1. The HOMO of $[3]^-$ is a cobalt-centered d_{z^2} orbital, which indicates that $[3]^0$ is reduced at cobalt to form Co(I). This observation is consistent with previous calculations performed with BLYP indicating a cobalt-centered d_{z^2} lowest unoccupied molecular orbital of $[3]^0$.[58] The HOMO of $[3]^{2-}$ has mixed metal/ligand character, suggesting that $[3]^-$ is reduced equally at both the metal and the porphyrin, forming Co("0.5"). This characterization differs from our previous calculations on the nickel analogue of [3] indicating that the singly occupied molecular orbital (SOMO) of the monoanion is σ^* $d_{x^2-y^2}$ on the nickel and the highest SOMO of the triplet dianion is nearly entirely ligand based.[59] For both cobalt and nickel, the HOMO of the lowest-energy dianion has some ligand character, breaking the aromaticity in the porphyrin ring.

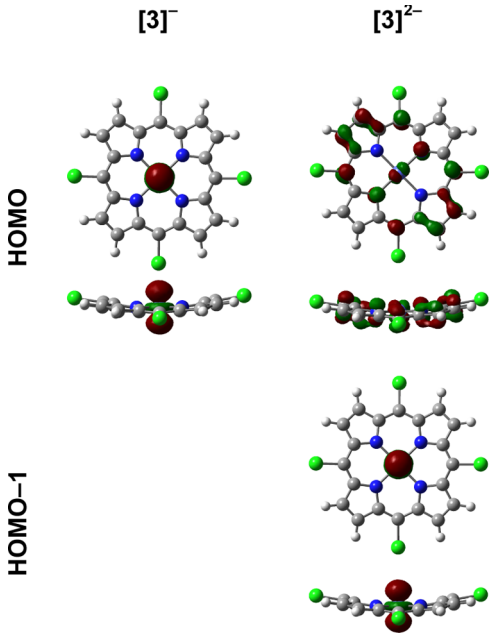

Figure 1. Top (upper structures) and side (lower structures) views of HOMOs of $[3]^-$ and $[3]^{2-}$ and HOMO-1 of $[3]^{2-}$ (isovalue 0.05). The HOMO of $[3]^-$ and the HOMO-1 of $[3]^{2-}$, corresponding to the paired α spin orbital, have d_{z^2} character. The HOMO of $[3]^{2-}$, corresponding to the unpaired α spin orbital, has mixed metal−ligand character. Color scheme: purple, Co; blue, N; gray, C; green, Cl; white, H.

Relative free energies of protonated $[3]^-$ and $[3]^{2-}$ were calculated for three proton acceptor sites: the cobalt center, a pyrrolic nitrogen, and a carbon at the *meso* position of the ring (Table 1 and Table S6 (Supporting Information)). The three protonated species are denoted $[3\text{-}H_{Co}]$, $[3\text{-}H_N]$, and $[3\text{-}H_C]$ for protonation at cobalt, nitrogen, and carbon, respectively. $[3\text{-}H]^0$, which corresponds to protonated $[3]^-$, is most stable when protonated at the cobalt center ($[3\text{-}H_{Co}]^0$) as a singlet. $[3\text{-}H]^-$, which corresponds to protonated $[3]^{2-}$, is most stable when protonated at the *meso* carbon, forming the phlorin complex $[3\text{-}H_C]^-$. Note that the aromaticity in the porphyrin ring of Co("0.5") in $[3]^{2-}$ is already broken because the unpaired electron is shared nearly equally by the metal and ligands. Formation of a phlorin stabilizes the remaining conjugation in the ring. Due to the puckering of the porphyrin ring, two protonated structures are possible when protonating at the *meso* carbon, and both structures were considered.

Table 1. Calculated Relative Free Energies and Spin Densities on Cobalt for [3-H]

complex	S^a	rel free energy^b	$\rho_{Co}{}^c$
$[3\text{-}H_{Co}]^0$	0	0.00	0.00
$[3\text{-}H_N]^0$	0	15.4	0.00
$[3\text{-}H_C]^{0\,d}$	0	13.3	0.00
$[3\text{-}H_{Co}]^0$	1	32.3	0.19
$[3\text{-}H_N]^0$	1	20.9	1.30
$[3\text{-}H_C]^{0\,d}$	1	4.3	1.05
$[3\text{-}H_{Co}]^-$	1/2	0.00	0.03
$[3\text{-}H_N]^-$	1/2	13.4	0.47
$[3\text{-}H_C]^{-\,d}$	1/2	−12.2	0.96

^{a}*S* indicates the total spin of the system. ^{b}Free energies in kcal/mol relative to the closed-shell singlet $[3\text{-}H_{Co}]^0$ for the neutral species and $[3\text{-}H_{Co}]^-$ for the monoanions. ^{c}Mulliken spin density on Co. ^{d}Geometry in which the proton binds from the top. When the proton binds from the bottom, the relative free energy of singlet $[3\text{-}H_C]^0$ is 7.9 kcal/mol, and the chlorine atom dissociates for triplet $[3\text{-}H_C]^0$ and for $[3\text{-}H_C]^-$.

H_2 evolution mechanisms by [3] can be analyzed from the calculated reduction potentials and pK_as of the relevant intermediates. Selected calculated pK_as are given in Table 2, and the calculated reduction potentials are given in Table 3. Additional relative pK_as and reduction potentials calculated from structures optimized in the gas phase are provided in Tables S12−S15 (Supporting Information). The agreement between the calculated and experimental reduction potentials provides validation of the computational methodology. Cyclic voltammograms (CVs) of [3] showed that the second reduction peak ($E_{1/2}$ = −1.98 V vs Fc^+/Fc) becomes catalytic upon addition of benzoic acid (pK_a = 20.7 in acetonitrile).[25] On

dx.doi.org/10.1021/cs501454y | ACS Catal. 2014, 4, 4516−4526

Table 2. Calculated Relative pK_as[a]

complex	pK_a
[**1**-***H***]^0	*20.2* (20.2)[b]
[**1**-***H***]$^-$	22.3
[**1**-***H***]$^{2-}$	22.5
[**1**-***H***$_{Co}$]$^-$	16.6
[**1**-***H***$_{Co}$]$^{2-}$	22.5
[**1**-***H***$_C$]$^-$	12.2
[**1**-***H***$_C$]$^{2-}$	31.0
[**3**-***H***$_{Co}$]^0	*15.0* (8.0−20.7)[c]
[**3**-***H***$_{Co}$]$^-$	24.1 (>20.7)[c]
[**3**-***H***$_C$]^0	9.2
[**3**-***H***$_C$]$^-$	33.1
[**3**-H$_C$***H***$_{Co}$]^0	10.6
[**3**-H$_C$***H***$_{Co}$]$^-$	27.6
[**1**-H***H***$_{Co}$]^0	16.2 (8.0−20.7)[c]
[**1**-H***H***$_{Co}$]$^-$	24.9 (>20.7)[c]
[**1**-H***H***$_C$]^0	10.5
[**1**-H***H***$_C$]$^-$	30.5
[**1**-H$_C$***H***$_{Co}$]^0	3.3
[**1**-H$_C$***H***$_{Co}$]$^-$	14.4
[**1**-***H***H$_C$]^0	20.6
[**1**-***H***H$_C$]$^-$	22.0

[a]Calculated relative pK_as are given in acetonitrile for the deprotonation of the italicized proton relative to the pK_a of [**1**-***H***]^0 or [**3**-***H***$_{Co}$]^0. (See Computational Methods for an explanation of the choice of references.) The experimental values are given in parentheses. The italicized calculated pK_as were used as references and agree with experiment by construction. [b]Experiment from ref 51. [c]Estimate from experimental range in ref 24.

Table 3. Calculated Reduction Potentials[a]

ox	red	$E°$	mechanism
[**3**]^0	[**3**]$^-$	−*1.00* (−1.00)[b]	
[**3**]$^-$	[**3**]$^{2-}$	−1.98 (−1.98)	
[**2**]^0	[**2**]$^-$	−1.01 (−1.10)	
[**2**]$^-$	[**2**]$^{2-}$	−2.10 (−2.14)	
[**1**-**H**]^0	[**1**-**H**]$^-$	−1.03 (−1.08)	
[**1**-**H**]$^-$	[**1**-**H**]$^{2-}$	−2.00	ET-PT
[**1**-**H**]$^-$	[**1**-**H**$_{Co}$]$^{2-}$	−2.00	concerted
[**1**-**H**]$^-$	[**1**-**H**$_N$]$^{2-}$	−2.50	concerted
[**1**-**H**]$^-$	[**1**-**H**$_C$]$^{2-}$ [c]	−1.50	concerted
[**1**-**H**$_{Co}$]$^-$	[**1**-**H**$_{Co}$]$^{2-}$	−1.66	PT-ET
[**1**-**H**$_N$]$^-$	[**1**-**H**$_N$]$^{2-}$	−2.35	PT-ET
[**1**-**H**$_C$]$^-$ [c]	[**1**-**H**$_C$]$^{2-}$ [c]	−0.90	PT-ET
[**3**-**H**$_{Co}$]^0	[**3**-**H**$_{Co}$]$^-$	−1.44	
[**3**-**H**$_C$]$^-$	[**3**-**H**$_C$]$^{2-}$	−1.61	
[**3**-**H**$_C$**H**$_{Co}$]$^-$	[**3**-**H**$_C$**H**$_{Co}$]$^{2-}$	−1.96	
[**1**-**HH**$_{Co}$]^0	[**1**-**HH**$_{Co}$]$^-$	−1.49 (−1.5)	
[**1**-**HH**$_C$]$^-$	[**1**-**HH**$_C$]$^{2-}$	−1.65	

[a]Values are given in volts vs Fc$^+$/Fc in acetonitrile. Experimental values of $E_{1/2}$ are given in parentheses, as obtained from ref 50 for [**3**] and ref 24 for [**1**-**H**] and [**2**]. [b]$E_{1/2}$([**3**]^0/[**3**]$^-$) was used as the reference and agrees by construction. [c]The value is for the geometry without the large structural rearrangement. With the large structural rearrangement, $E°$([**1**-**H**]$^-$/[**1**-**H**$_C$]$^{2-}$) = −1.51 V vs Fc$^+$/Fc for the concerted mechanism and is the same to within the numerical accuracy given for the PT-ET mechanism. Thus, the values for the two geometries are the same to within the accuracy of the computational method.

the basis of our calculations, Co("0.5") in [**3**]$^{2-}$ would become protonated predominantly at the *meso* carbon to form [**3**-**H**$_C$]$^-$ (pK_a = 33), although it is thermodynamically favorable for [**3**-**H**$_{Co}$]$^-$ to be formed as well (pK_a = 24). With a sufficiently strong acid, Co(I) in [**3**]$^-$ could become protonated to form a Co(III) hydride intermediate, [**3**-**H**$_{Co}$]^0.

Figure 2 presents the experimental CVs for [**1**-**H**] and [**2**] in the absence of external acid as well as in the presence of

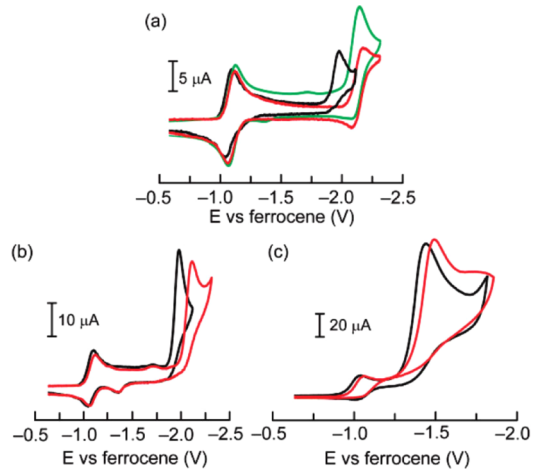

Figure 2. (a) CVs of 0.5 mM [**1**-**H**] (black line), [**2**] (red line), and [**2**] in the presence of 0.5 mM benzoic acid (green line) in acetonitrile. (b) CVs of 0.5 mM [**1**-**H**] in the presence of 2.5 mM benzoic acid (black line) and 0.5 mM [**2**] in the presence of 3.0 mM benzoic acid (red line) in acetonitrile. (c) CVs of 0.8 mM [**1**-**H**] (black line) and [**2**] (red line) in the presence of 10 mM tosic acid. Reproduced with permission from ref 24. Copyright 2011 American Chemical Society.

benzoic acid or tosic acid. For [**1**-**H**] and [**2**], addition of tosic acid (pK_a = 8.0 in acetonitrile)[52] gives rise to a new catalytic peak at ca. −1.5 V vs Fc$^+$/Fc in cyclic voltammetry (depicted in Figure 2c), proposed to be the Co(III/II) hydride peak.[24] The calculated reduction potential $E°$([**3**-**H**$_{Co}$]^0/[**3**-**H**$_{Co}$]$^-$) = −1.44 V vs Fc$^+$/Fc is consistent with the Co(III/II) hydride assignment in these complexes. Free energy diagrams for thermodynamically favorable H_2 evolution catalyzed by [**3**] with tosic and benzoic acid are provided in Figures S4 and S5 (Supporting Information), respectively.

Electronic Structure and Characterization of [1-H]. The complex [**1**-**H**] differs from [**3**] in that one pentafluorophenyl group is replaced with a xanthene group that contains the hangman moiety. The calculated spin densities on Co for [**1**-**H**]^0 and [**1**-**H**]$^{2-}$, which are both doublets, are 1.06 and 0.42, respectively. These spin densities are very similar to those calculated for [**3**]^0 and [**3**]$^{2-}$ (1.00 and 0.40, respectively). Because of the presence of the xanthene group, the puckering of the porphyrin ring of [**1**-**H**] can adopt two structural minima not present in [**3**]. The global minima for [**1**-**H**]^0 and [**1**-**H**]$^-$ correspond to the porphyrin ring puckered upward ($\Delta G°$ = −0.5 and −0.1 kcal/mol, respectively), while the global minimum for [**1**-**H**]$^{2-}$ corresponds to the porphyrin ring puckered downward ($\Delta G°$ = −1.3 kcal/mol). Additional local minima ($\Delta G°$ = ∼3−4 kcal/mol for each puckering conformation) were found in which the proton in the hanging moiety is positioned over the porphyrin ring instead of pointing toward the xanthene ether oxygen. Figure 3 depicts optimized structures of [**1**-**H**]$^-$ (puckered upward) and [**1**-**H**]$^{2-}$ (puckered downward) with the proton pointing toward the xanthene ether oxygen or hanging over the porphyrin ring. The puckering of the ring and the position of the hanging proton

dx.doi.org/10.1021/cs501454y | ACS Catal. 2014, 4, 4516−4526

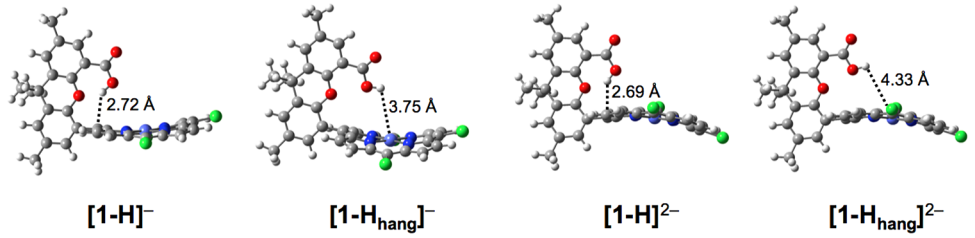

Figure 3. Optimized structures of $[\mathbf{1}\text{-H}]^-$ with the porphyrin ring puckered upward and $[\mathbf{1}\text{-H}]^{2-}$ with the porphyrin ring puckered downward. The global minimum for each species is the structure with the proton pointing toward the xanthene ether oxygen with the porphyrin ring puckering shown here. The H−C and H−Co distances are provided for the structures with the carboxylic acid proton pointing toward the xanthene ether oxygen (left) and hanging over the porphyrin ring (right), respectively, for each species. The associated O−C and O−Co distances are given in the main text. Color scheme: purple, Co; blue, N; gray, C; green, Cl; red, O; white, H.

may affect the identity of the proton acceptor and the structure of $[\mathbf{1}\text{-H}]$ after intramolecular PT. Note that all of these minima may be thermally accessible at 298.15 K, although the equilibrium populations of the minima with the carboxylic acid proton positioned over the porphyrin rings will be 150−850 times lower than those with the proton pointing toward the xanthene ether oxygen for both puckering conformations.

We explored three proton acceptor sites: the cobalt center, a pyrrolic nitrogen, and a carbon at the *meso* position of the ring. The calculated proton donor−acceptor distances and donor−proton−acceptor angles for the global and local minima of $[\mathbf{1}\text{-H}]^-$, which is the relevant species for both the sequential PT-ET mechanism and the concerted PCET mechanism, are given in Table S8 (Supporting Information). Intramolecular PT is favored in geometries with a short equilibrium proton donor−acceptor distance. In the global minimum geometry, the ideal proton acceptor candidate is the *meso* carbon, which has a proton donor−acceptor distance of 3.54 Å. The donor−proton−acceptor angle is also the most linear at 139.6°. If the proton were to transfer to the cobalt or a pyrrolic nitrogen, the proton would most likely need to be positioned over the porphyrin ring, as in the local minimum geometry $[\mathbf{1}\text{-H}_{\mathbf{hang}}]^-$ (ΔG° = +3.1 kcal/mol) depicted in Figure 3. In this local minimum geometry, PT to the cobalt center as well as to the two pyrrolic nitrogen atoms farthest from the xanthene becomes more probable due to the decrease in the proton donor−acceptor distance and increase in the donor−proton−acceptor angle. The H−C and H−Co distances with the proton pointing toward the xanthene ether oxygen and hanging over the porphyrin ring, respectively, are shown in Figure 3 for $[\mathbf{1}\text{-H}]^-$ and $[\mathbf{1}\text{-H}]^{2-}$.

The proton donor−acceptor distances and donor−proton−acceptor angles for the global and local minima of $[\mathbf{1}\text{-H}]^{2-}$, the relevant species for the sequential ET-PT mechanism, are given in Table S9 (Supporting Information). Similar to $[\mathbf{1}\text{-H}]^-$, the global minimum of $[\mathbf{1}\text{-H}]^{2-}$ favors transfer of the proton to the nearest *meso* carbon, which has the shortest proton donor−acceptor distance (3.51 Å) and the most linear donor−proton−acceptor angle (139.6°). Adoption of the local minimum in which the proton is hanging over the porphyrin ring (ΔG° = +3.9 kcal/mol) does not drastically improve the proton donor−acceptor interface for any of the remaining acceptors. Thus, for any of the proposed mechanisms, structural features of the hangman moiety suggest that the likely proton acceptor is the closest *meso* carbon.

The relative free energies and spin densities on Co of $[\mathbf{1}\text{-H}]$ after intramolecular PT, denoted $[\mathbf{1}\text{-H}_{\mathbf{Co}}]$, $[\mathbf{1}\text{-H}_{\mathbf{N}}]$, and $[\mathbf{1}\text{-H}_{\mathbf{C}}]$ for cobalt, nitrogen, and carbon acceptors, respectively, were also calculated for the monoanion and dianion (Table 4 and Table S10 (Supporting Information)). For the monoanion, the proton is most stable on the nitrogen acceptor ($[\mathbf{1}\text{-H}_{\mathbf{N}}]^-$) as a singlet, although this species is still higher in free energy than if the proton had remained on the oxygen acceptor ($[\mathbf{1}\text{-H}]^-$; ΔG°_{PT} = +3.4 kcal/mol). For the dianion, the proton is most stable on the carbon acceptor ($[\mathbf{1}\text{-H}_{\mathbf{C}}]^{2-}$; ΔG°_{PT} = −11.6 kcal/mol), and the spin density on Co is approximately unity. As in the case for [**3**], two different structures are possible following PT. When the porphyrin ring is puckered downward, a large structural rearrangement occurs in which the porphyrin ring bends away from the hangman moiety. When the porphyrin ring is puckered upward, this structural rearrangement does not occur. The latter structure is 0.4 kcal/mol lower in free energy than the former structure. Most importantly, the phlorin $[\mathbf{1}\text{-H}_{\mathbf{C}}]^{2-}$ is the global minimum for the doubly reduced species (ΔG°_{PT} = −11.6 kcal/mol), while $[\mathbf{1}\text{-H}_{\mathbf{Co}}]^{2-}$ has a free energy nearly identical with that of $[\mathbf{1}\text{-H}]^{2-}$ (ΔG°_{PT} = −0.02 kcal/mol).

Table 4. Calculated Relative Free Energies and Spin Densities on Cobalt for $[\mathbf{1}\text{-H}]$ after Intramolecular Proton Transfer

complex	S^a	rel free energy^b	$\rho_{Co}{}^c$
$[\mathbf{1}\text{-H}_{\mathbf{Co}}]^-$	0	7.8	0.00
$[\mathbf{1}\text{-H}_{\mathbf{N}}]^-$	0	3.4	0.00
$[\mathbf{1}\text{-H}_{\mathbf{C}}]^{-\,d}$	0	18.4	0.00
$[\mathbf{1}\text{-H}_{\mathbf{C}}]^{-\,e}$	0	21.9	0.00
$[\mathbf{1}\text{-H}_{\mathbf{Co}}]^-$	1	42.2	0.19
$[\mathbf{1}\text{-H}_{\mathbf{N}}]^-$	1	20.9	1.35
$[\mathbf{1}\text{-H}_{\mathbf{C}}]^{-\,d}$	1	14.2	1.09
$[\mathbf{1}\text{-H}_{\mathbf{C}}]^{-\,e}$	1	13.8	1.17
$[\mathbf{1}\text{-H}_{\mathbf{Co}}]^{2-}$	1/2	−0.02	0.04
$[\mathbf{1}\text{-H}_{\mathbf{N}}]^{2-}$	1/2	11.4	0.47
$[\mathbf{1}\text{-H}_{\mathbf{C}}]^{2-\,d}$	1/2	−11.2	0.99
$[\mathbf{1}\text{-H}_{\mathbf{C}}]^{2-\,e}$	1/2	−11.6	1.08

^{a}S indicates the total spin of the system. ^{b}Free energies are given in kcal/mol relative to the closed-shell singlet $[\mathbf{1}\text{-H}]^-$ for the monoanions and $[\mathbf{1}\text{-H}]^{2-}$ for the dianions. ^{c}Mulliken spin density on Co. ^{d}Geometry with large structural rearrangement. ^{e}Geometry without large structural rearrangement.

To determine if residual water may impact the thermodynamics, we also performed calculations with an explicit water molecule that can hydrogen bond with the hangman moiety and thereby potentially facilitate proton transfer (Table S11 (Supporting Information)). The relative free energies of the monoanion and dianion Co hydrides and phlorin complexes

dx.doi.org/10.1021/cs501454y | ACS Catal. 2014, 4, 4516−4526

changed by at most 1.5 kcal/mol in the presence of a water molecule. Thus, the addition of water has little effect on the thermodynamics of cobalt hydride formation. Qualitatively, the only difference that arises due to the addition of water is the energetic ordering of the local minima that differ in the position of the carboxylic acid proton of the hangman moiety. When a water molecule is present, the carboxylic acid proton is more stable when it is positioned over the porphyrin ring because it can readily hydrogen bond with the water molecule, whereas when a water molecule is not present, it is more stable when it is positioned toward the xanthene ether oxygen.

The calculated reduction potentials of the Co porphyrins are provided in Table 3. This table includes the reduction potentials of [**2**], which behaves electrochemically similarly to [**1-H**] but lacks the proton relay. The excellent agreement with experimentally measured reduction potentials provides further validation of the computational methods. For [**1-H**], the reduction potentials were calculated for the structures before and after intramolecular PT as well as for concerted PCET. The reduction potential before PT, $E^\circ([\mathbf{1\text{-}H}]^-/[\mathbf{1\text{-}H}]^{2-}) = -2.00$ V vs Fc^+/Fc, is equivalent to the reduction potential for concerted PCET to the metal center, $E^\circ([\mathbf{1\text{-}H}]^-/[\mathbf{1\text{-}H_{Co}}]^{2-})$, because the dianionic products have nearly identical free energies. For the concerted PCET mechanism, $E^\circ([\mathbf{1\text{-}H}]^-/[\mathbf{1\text{-}H_N}]^{2-}) = -2.50$ V vs Fc^+/Fc is very negative due to the high free energy $[\mathbf{1\text{-}H_N}]^{2-}$ product, and $E^\circ([\mathbf{1\text{-}H}]^-/[\mathbf{1\text{-}H_C}]^{2-}) = -1.50$ V vs Fc^+/Fc is more positive due to the stability of the $[\mathbf{1\text{-}H_C}]^{2-}$ phlorin product. For the PT-ET mechanism, $E^\circ([\mathbf{1\text{-}H_C}]^-/[\mathbf{1\text{-}H_C}]^{2-}) = -0.90$ V vs Fc^+/Fc (for either conformer) is very positive because the oxidized state $[\mathbf{1\text{-}H_C}]^-$ is the product of a thermodynamically unfavorable PT. These reduction potentials will be analyzed in the context of possible PCET mechanisms in the next subsection.

PCET Mechanism of [1-H]. The PCET mechanism of [**1-H**] was previously investigated with experimental and simulated CVs.[25] The hypothesis that PCET proceeds via the ET-PT mechanism was studied by analysis of the catalytic peak potential, E_p, which has the following form for a fast, reversible ET followed by intramolecular PT:

$$E_p = E^\circ - 0.78\frac{RT}{F} + \frac{RT}{2F}\ln\left(\frac{RT}{F}\frac{k_{PT}}{\nu}\right) \quad (2)$$

where E° is the reversible potential of the ET step, k_{PT} is the proton transfer rate constant, and ν is the scan rate of the CV. If the mechanism is ET-PT, the plot of $(E_p - E^\circ)F/RT$ versus $\ln \nu$ should be linear with a slope of -0.5. Experimental CVs revealed a linear plot at low scan rates but a distinct curvature at high scan rates, which can be ascribed to kinetic competition between the ET and PT steps. The experimentally observed anodic shift of ~200 mV of the catalytic wave of [**1-H**] relative to [**2**] (depicted in Figure 2a by the black and red CVs), called the "hangman effect,"[30] arises from two distinct phenomena: the positive charge of the proton proximal to the metal center, which causes a shift in $E^\circ([\mathbf{1\text{-}H}]^-/[\mathbf{1\text{-}H}]^{2-})$ relative to $E^\circ([\mathbf{2}]^-/[\mathbf{2}]^{2-})$, and the effect of the ET-PT mechanism, which causes a shift in the peak position relative to $E^\circ([\mathbf{1\text{-}H}]^-/[\mathbf{1\text{-}H}]^{2-})$, as described by eq 2.[25]

The proton transfer rate constant, k_{PT}, was extracted from the simulated CVs that reproduced the experimental peak positions as a function of scan rate. Because the formally Co(I/0) couple of [**1-H**] is irreversible (Figure 2), the reduction potential $E^\circ([\mathbf{1\text{-}H}]^-/[\mathbf{1\text{-}H}]^{2-})$ was assumed to be similar to that of [**2**] in the CV simulations.[25] Our calculations show that the formal reduction potential $E^\circ([\mathbf{1\text{-}H}]^-/[\mathbf{1\text{-}H}]^{2-})$ is ~100 mV less negative than $E^\circ([\mathbf{2}]^-/[\mathbf{2}]^{2-})$ (Table 3). This shift in the thermodynamic reduction potential is most likely due to the presence of the proton proximal to the metal center. Additional CV simulations could be performed to determine the sensitivity of the extracted intramolecular PT rate constant to the thermodynamic reduction potential. In comparison to the experimental $E_{cat}[\mathbf{1}] \approx -1.9$ V vs Fc^+/Fc with benzoic acid (Figure 2b), our calculated $E^\circ([\mathbf{1\text{-}H}]^-/[\mathbf{1\text{-}H}]^{2-}) = -2.00$ V vs Fc^+/Fc implies an additional anodic shift of 100 mV in peak position due to the subsequent PT step, as described by eq 2. According to our calculated relative free energies of the dianion, PT is only thermodynamically favorable from $[\mathbf{1\text{-}H}]^{2-}$ to $[\mathbf{1\text{-}H_C}]^{2-}$ ($\Delta G^\circ = -11.6$ kcal/mol, $K_{eq} = 3.2 \times 10^8$ at 298.15 K).

To determine the rate constant of intramolecular PT from $[\mathbf{1\text{-}H}]^{2-}$ to $[\mathbf{1\text{-}H_C}]^{2-}$, which is thermodynamically favorable, we calculated the transition state structure. The porphyrin ring of the global minimum structure of $[\mathbf{1\text{-}H_C}]^{2-}$ ($S = 1/2$, spin density of 1.08 on Co) is puckered upward. We found a local minimum of $[\mathbf{1\text{-}H}]^{2-}$ that is similarly puckered upward and denote this local minimum structure $[\mathbf{1'\text{-}H}]^{2-}$ ($\Delta G^\circ = +1.3$ kcal/mol, $K_{eq} = 0.1$ at 298.15 K). The puckering of the porphyrin ring in $[\mathbf{1\text{-}H}]^{2-}$ does not affect the spin density on the cobalt ($\rho_{Co} = 0.42$ for both puckering configurations) according to the calculations. We calculated the transition state structure associated with PT from $[\mathbf{1'\text{-}H}]^{2-}$ to $[\mathbf{1\text{-}H_C}]^{2-}$. The resulting transition state structure, denoted $[\mathbf{1^\ddagger}]^{2-}$, has a single imaginary frequency of 1377 cm^{-1} that corresponds to the PT mode and a spin density of 0.59 on Co. The proton is positioned 1.22 Å from the donor oxygen and 1.51 Å from the acceptor carbon at a proton donor–acceptor distance of 2.69 Å and a donor–proton–acceptor angle of 161°. Following the intrinsic reaction coordinate (IRC) from this transition state structure leads to the minima corresponding to $[\mathbf{1'\text{-}H}]^{2-}$ and $[\mathbf{1\text{-}H_C}]^{2-}$. The free energy of $[\mathbf{1^\ddagger}]^{2-}$ is 9.0 kcal/mol higher than that of $[\mathbf{1'\text{-}H}]^{2-}$. According to transition state theory, the resulting PT rate constant is 1.4×10^6 s^{-1} at 298.15 K. This rate constant is consistent with the experimentally determined intramolecular PT rate constant of ca. 8.5×10^6 s^{-1}, which corresponds to an 8.0 kcal/mol free energy barrier.[25] The reaction free energy pathway for intramolecular PT from the carboxylic acid to the *meso* carbon in $[\mathbf{1\text{-}H}]^{2-}$ is depicted in Figure 4. Note that the free energy barrier for PT to the Co center is expected to be much larger on the basis of the H–Co distance of 4.33 Å, in contrast to the H–C distance of 2.69 Å at the global minimum.

The results of these computational studies are consistent with the experiments suggesting that the PCET reaction proceeds via an ET-PT mechanism. The PT-ET mechanism can be discounted due to the unfavorable thermodynamics of PT from the Co(I) species to certain potential proton acceptors (Table 4 and Table S10 (Supporting Information)), the structure of the proton donor–acceptor interface (Table S8 (Supporting Information)), and the subsequent reduction potentials (Table 3). Experimentally, $E_{cat}[\mathbf{1}] \approx -1.9$ V vs Fc^+/Fc with benzoic acid, which is anodically shifted ~200 mV from the Co(I/0) potential. Proton transfer to the carbon, $\Delta G^\circ([\mathbf{1\text{-}H}]^- \rightarrow [\mathbf{1\text{-}H_C}]^-) = \sim 14$ kcal/mol, is thermodynamically unfavorable. As a result, the subsequent reduction potential, $E^\circ([\mathbf{1\text{-}H_C}]^-/[\mathbf{1\text{-}H_C}]^{2-}) = -0.90$ V vs Fc^+/Fc, is artificially positive. Proton transfer to the cobalt,

dx.doi.org/10.1021/cs501454y | ACS Catal. 2014, 4, 4516–4526

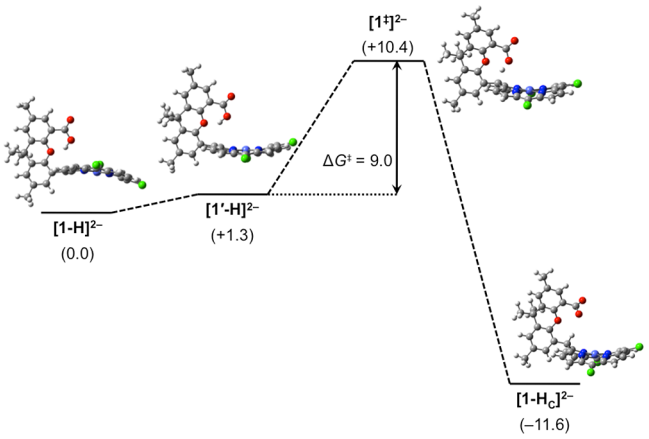

Figure 4. Calculated reaction free energy pathway for intramolecular PT of $[\mathbf{1}\text{-H}]^{2-}$. Free energies are given in kcal/mol relative to $[\mathbf{1}\text{-H}]^{2-}$. Ring puckering forms the local minimum $[\mathbf{1}'\text{-H}]^{2-}$, after which the proton transfers to generate $[\mathbf{1}\text{-H}_\mathbf{C}]^{2-}$ through the transition state $[\mathbf{1}^{\ddagger}]^{2-}$. Color scheme: purple, Co; blue, N; gray, C; green, Cl; red, O; white, H.

$\Delta G^\circ([\mathbf{1}\text{-H}]^- \rightarrow [\mathbf{1}\text{-H}_{Co}]^-)$ = 7.8 kcal/mol, is also thermodynamically unfavorable. The subsequent reduction potential, $E^\circ([\mathbf{1}\text{-H}_{Co}]^-/[\mathbf{1}\text{-H}_{Co}]^{2-})$ = −1.66 V vs Fc^+/Fc, is reasonable, although the proton donor−acceptor interface does not structurally favor formation of a cobalt hydride. Finally, proton transfer to a nitrogen, $\Delta G^\circ([\mathbf{1}\text{-H}]^- \rightarrow [\mathbf{1}\text{-H}_N]^-)$ = 3.4 kcal/mol, is thermodynamically accessible but is followed by reduction at $E^\circ([\mathbf{1}\text{-H}_N]^-/[\mathbf{1}\text{-H}_N]^{2-})$ = −2.35 V vs Fc^+/Fc, which is much too negative in comparison to the catalytic potential $E_{cat}[\mathbf{1}] \approx$ −1.9 V vs Fc^+/Fc with benzoic acid.

The concerted PCET reaction can also be excluded on the basis of our calculations. The calculated reduction potentials for concerted PCET from $[\mathbf{1}\text{-H}]^-$ to $[\mathbf{1}\text{-H}_\mathbf{C}]^{2-}$ or $[\mathbf{1}\text{-H}_N]^{2-}$ are −1.50 V vs Fc^+/Fc and −2.50 V vs Fc^+/Fc, respectively. The phlorin product is highly stabilized, leading to a reduction potential that is too positive in comparison to $E_{cat}[\mathbf{1}] \approx$ −1.9 V vs Fc^+/Fc with benzoic acid, whereas the nitrogen acceptor product is highly destabilized, leading to a reduction potential that is too negative. Concerted PCET from $[\mathbf{1}\text{-H}]^-$ to $[\mathbf{1}\text{-H}_{Co}]^{2-}$ (E° = −2.00 V vs Fc^+/Fc) is unlikely, due to the long proton donor−acceptor distance (O−Co = 4.21 Å), as the rate constant of concerted PCET is proportional to the square of the overlap integral between the proton vibrational wave functions localized on the proton donor and acceptor, respectively.[6,9] Thus, although electrochemical PCET rate theory[6,14,60] could be used to analyze the kinetics of the concerted PCET mechanism, the calculated reduction potentials and structural characteristics are not consistent with this mechanism.

Hydrogen Evolution by [1-H]. Experimental studies have shown that [**1**-H] and [**2**] evolve H_2 at ca. −1.5 V vs Fc^+/Fc with tosic acid and at more negative potentials (−1.9 V vs Fc^+/Fc and −2.1 V vs Fc^+/Fc, respectively) with benzoic acid, as depicted in Figure 2. Complex [**2**] lacks an internal proton relay and is thus expected to evolve H_2 in a fashion similar to that for [**3**]. The precise mechanism for H_2 evolution by [**1**-H], however, is complicated by the "hangman" moiety of the xanthene backbone. The calculated free energy diagrams for H_2 evolution by [**1**-H] and a complete mechanistic cycle are depicted in Figure 5.

The top left of Figure 5 corresponds to the reaction with benzoic acid and an applied potential of −1.9 V vs Fc^+/Fc. In this case, after the PCET reaction discussed above (steps 2 and 3 in Figure 5), the resulting dianionic phlorin $[\mathbf{1}\text{-H}_\mathbf{C}]^{2-}$ can become protonated at the carboxylate from benzoic acid to form the doubly protonated $[\mathbf{1}\text{-HH}_\mathbf{C}]^-$ (step 4). Note that the calculated pK_a is 22.0 for deprotonation of the carboxylate in $[\mathbf{1}\text{-HH}_\mathbf{C}]^-$ and is 14.4 for deprotonation of Co in $[\mathbf{1}\text{-H}_\mathbf{C}\text{H}_{Co}]^-$ (Table 2). Because the pK_a of benzoic acid is 20.7, the carboxylate is much more likely to become protonated than the Co of $[\mathbf{1}\text{-H}_\mathbf{C}]^{2-}$. The calculated reduction potential of this species, $[\mathbf{1}\text{-HH}_\mathbf{C}]^-$, is −1.65 V vs Fc^+/Fc, which is less negative than the experimental catalytic potential $E_{cat}[\mathbf{1}] \approx$ −1.9 V vs Fc^+/Fc with benzoic acid and will occur spontaneously (step 5). At this point the free energy diagram branches into two possible pathways that involve either direct H_2 elimination (step 5′) or another reduction followed by H_2 elimination (steps 5 and 6). The calculated free energies for H_2 elimination from $[\mathbf{1}\text{-HH}_\mathbf{C}]^-$ (step 5′) and $[\mathbf{1}\text{-HH}_\mathbf{C}]^{2-}$ (step 6) are 5.7 and −5.9 kcal/mol, respectively. The H−H distance is 1.95 Å for both species; although this H−H distance is relatively long, thermal fluctuations of the molecule will enable sampling of shorter distances. Following the latter pathway, protonation of the carboxylate of $[\mathbf{1}]^{2-}$ (step 7) closes the catalytic cycle, re-forming $[\mathbf{1}\text{-H}]^-$. Following the former pathway, protonation of $[\mathbf{1}]^-$ (step 8′) closes the catalytic cycle, re-forming $[\mathbf{1}\text{-H}]^0$. The pathway that involves $[\mathbf{1}\text{-HH}_\mathbf{C}]^{2-}$ (steps 5−7) is more thermodynamically favorable than the pathway that involves $[\mathbf{1}\text{-HH}_\mathbf{C}]^-$ (steps 5′ and 8′) or than the pathway that requires oxidation of $[\mathbf{1}]^{2-}$ to $[\mathbf{1}]^-$ (step 7′; ΔG° = +17.3 kcal/mol at the applied potential). The proposed mechanistic cycle for H_2 evolution by [**1**-H] and benzoic acid, in conjunction with the formal oxidation states of the metal and formal charges of the ligands of the intermediates, is summarized in Figure 6.

The top right of Figure 5 corresponds to the reaction with tosic acid and an applied potential of −1.49 vs Fc^+/Fc. As for [**2**] and [**3**], addition of tosic acid to [**1**-H] results in protonation of $[\mathbf{1}\text{-H}]^-$ at the Co center, forming $[\mathbf{1}\text{-HH}_{Co}]^0$ (step 9). This species can be reduced at a less negative catalytic potential of $E^\circ([\mathbf{1}\text{-HH}_{Co}]^0/[\mathbf{1}\text{-HH}_{Co}]^-)$ = −1.49 V vs Fc^+/Fc (step 10) to evolve hydrogen with tosic acid (ΔG° = −18.5 kcal/mol, step 11). Note that protonation of $[\mathbf{1}\text{-H}]^-$ by tosic acid is more thermodynamically favorable at the Co center than at the *meso* carbon, as indicated by the calculated pK_as for deprotonation of $[\mathbf{1}\text{-HH}_{Co}]^0$ at the Co center (16.2, Table 2) and for deprotonation of $[\mathbf{1}\text{-HH}_\mathbf{C}]^0$ at the carbon (10.5, Table 2).

CONCLUSIONS

This paper presents a theoretical analysis of a series of cobalt porphyrins, focusing on the impact of the electronic structure on the HER mechanism. The Co(II) porphyrin $[\mathbf{3}]^0$ is electrochemically reduced to the Co(I) porphyrin $[\mathbf{3}]^-$. The ^{1}H NMR spectrum of the chemically reduced tetrabutylammonium salt $\mathbf{TBA}^+[\mathbf{3}]^-$ exhibits a sharp proton peak in the aromatic region, consistent with a diamagnetic Co(I) complex. Subsequent reduction produces a formally Co(0) complex with substantial ligand-based reduction. Calculations indicate that the unpaired electron in the doubly reduced species occupies a molecular orbital with nearly equal contributions from the Co center and the ligands. In contrast to the nickel analogue of [**3**], for which the formally Ni(0) intermediate is a triplet, the monoanionic and dianionic states of [**3**] remain low spin.

dx.doi.org/10.1021/cs501454y | ACS Catal. 2014, 4, 4516−4526

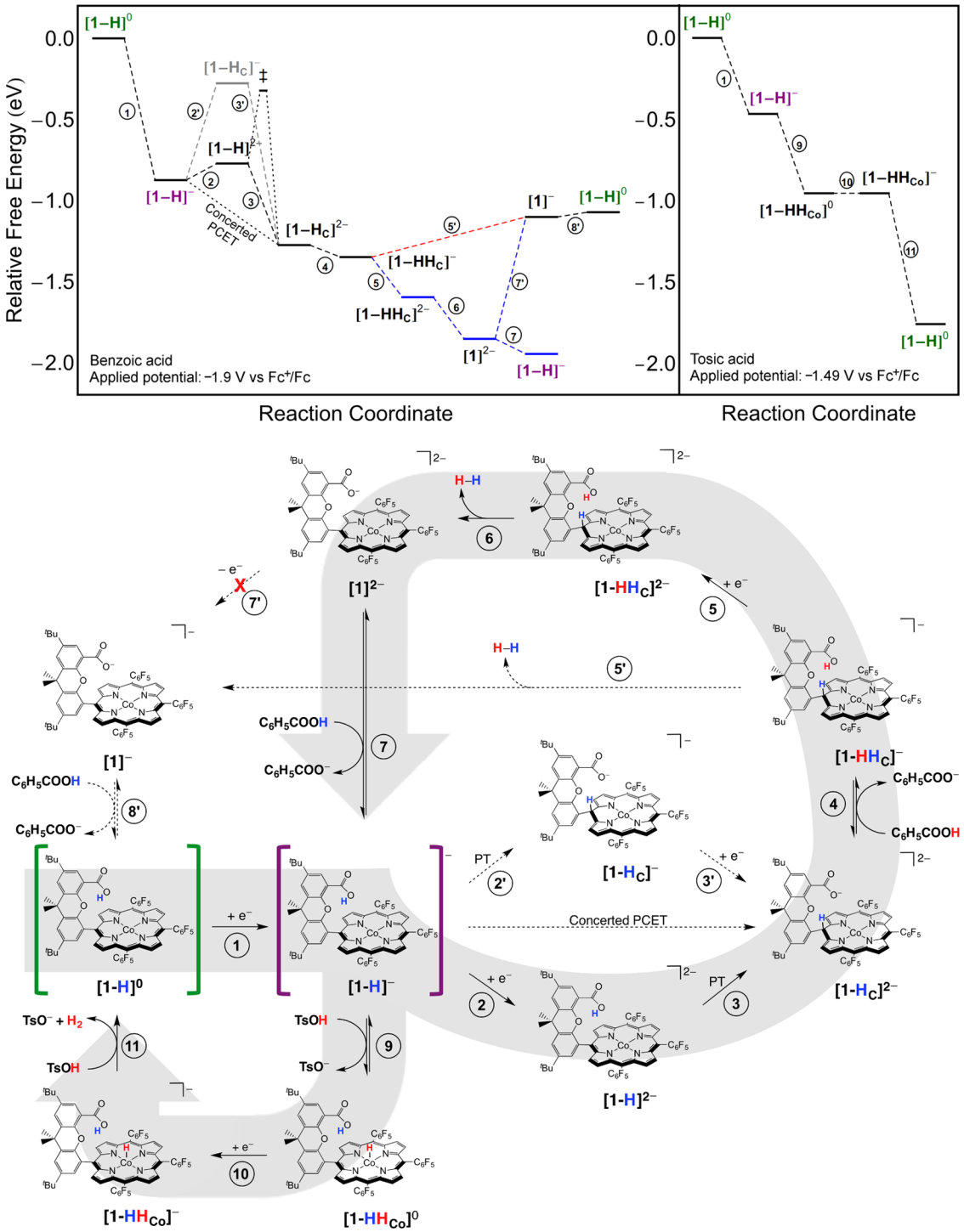

Figure 5. Free energy diagrams (top) for H_2 production catalyzed by [**1**-**H**] with benzoic acid (C_6H_5COOH, pK_a = 20.7)[53] and an applied potential of −1.9 V vs Fc^+/Fc (left) and tosic acid (TsOH, pK_a = 8.0)[52] with an applied potential of −1.49 V vs Fc^+/Fc (right). Complete mechanistic cycle of proposed mechanisms (bottom), where solid arrows indicate thermodynamically favorable pathways and dotted arrows represent thermodynamically unfavorable pathways. The proposed catalytic pathways with weak and strong acids follow the gray arrows in the background of the full catalytic cycle. The catalytic cycle starts with $[\mathbf{1}\text{-}\mathbf{H}]^0$ (shown in green) and is reduced (step 1) to $[\mathbf{1}\text{-}\mathbf{H}]^-$ (shown in purple). With benzoic (weak) acid, the mechanism continues with a PCET step. The proposed PCET mechanism is the sequential ET-PT mechanism (steps 2–3). The intramolecular PT barrier is labeled ‡ in the free energy diagram (top left), and the alternative sequential PT-ET mechanism (steps 2′ and 3′) is shown in gray. The carboxylate of $[\mathbf{1}\text{-}\mathbf{H}_\mathbf{C}]^{2-}$ is protonated (step 4) to form the doubly protonated $[\mathbf{1}\text{-}\mathbf{HH}_\mathbf{C}]^-$. Self-elimination of H_2 from $[\mathbf{1}\text{-}\mathbf{HH}_\mathbf{C}]^-$ (step 5′) is thermodynamically unfavorable, necessitating the reduction to $[\mathbf{1}\text{-}\mathbf{HH}_\mathbf{C}]^{2-}$ (step 5) before H_2 elimination (step 6). The deprotonated $[\mathbf{1}]^{2-}$ is protonated by acid to form $[\mathbf{1}\text{-}\mathbf{H}]^-$ and close the catalytic cycle in step 7. Oxidation of $[\mathbf{1}]^{2-}$ to $[\mathbf{1}]^-$ (step 7′) is very thermodynamically unfavorable (denoted with a red "X") at the applied catalytic potential (ΔG° = +17.3 kcal/mol). If $[\mathbf{1}]^-$ were formed, it could be protonated to form $[\mathbf{1}\text{-}\mathbf{H}]^0$ (step 8′) to close the catalytic cycle. With tosic (strong) acid, $[\mathbf{1}\text{-}\mathbf{H}]^-$ (shown in purple) is protonated at the Co center (step 9), forming the doubly protonated Co(III) hydride $[\mathbf{1}\text{-}\mathbf{HH}_\mathbf{Co}]^0$. After further reduction (step 10), H_2 is evolved with tosic acid (step 11).

dx.doi.org/10.1021/cs501454y | ACS Catal. 2014, 4, 4516−4526

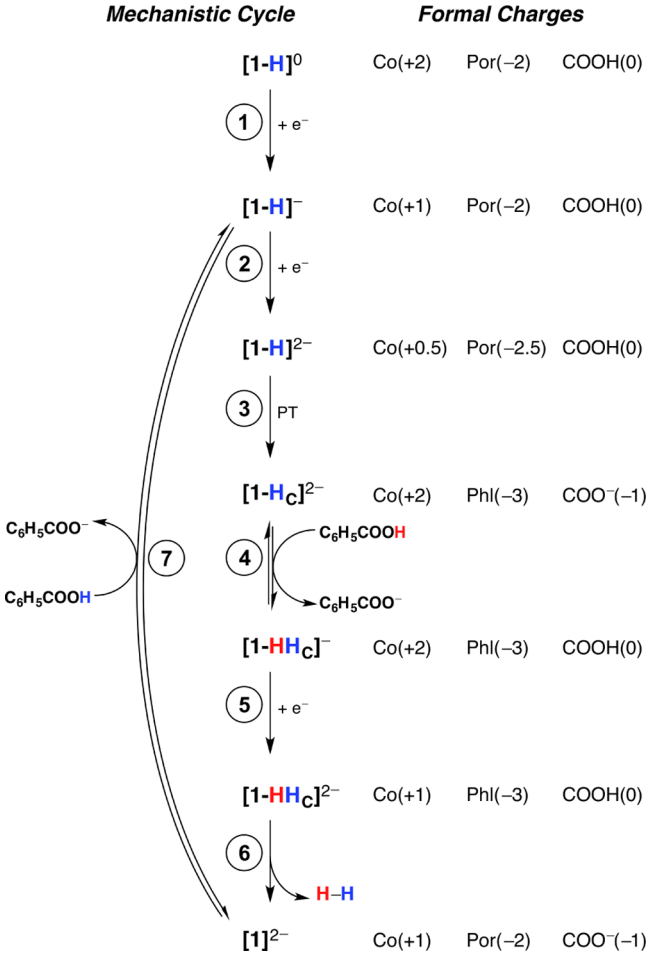

Figure 6. Proposed mechanistic cycle of H_2 evolution catalyzed by [**1**-H] with benzoic acid (left) and formal charges of the intermediates (right). The formal oxidation state of the metal center (Co) and formal charges of the porphyrin ring (Por), phlorin (Phl), carboxylic acid (COOH), and carboxylate (COO^-) are shown.

Formally Co(0) and Ni(0) porphyrin complexes both display some metal(I) character, indicating a significant degree of ligand noninnocence.

These properties of the electronic structure have mechanistic implications, owing to the broken aromaticity in the porphyrin ring of $[\mathbf{3}]^{2-}$. In particular, the ligand dearomatization affects the thermodynamics of the various protonated species. The Co(III) hydride structure $[\mathbf{3}\text{-}\mathbf{H}_{Co}]^0$ was found to be most stable upon protonation of $[\mathbf{3}]^-$, whereas the phlorin product $[\mathbf{3}\text{-}\mathbf{H}_C]^-$ was found to be most stable upon protonation of $[\mathbf{3}]^{2-}$. For $[\mathbf{3}]^-$, which is in the Co(I) oxidation state, protonation at the *meso* carbon would result in breaking the porphyrin aromaticity. For $[\mathbf{3}]^{2-}$, formulated as a mixed Co(I)/Co(0) species with a partially reduced porphyrin ligand, the aromaticity is already broken, and the formation of a phlorin stabilizes the remaining conjugation in the macrocycle.

The related hangman porphyrin [**1**-H], which is enhanced with a proton relay, was found to exhibit similar behavior. Specifically, the formally Co(0) $[\mathbf{1}\text{-H}]^{2-}$ is a mixed Co(I)/Co(0) species with partial ligand reduction. In this case, the HER mechanism is thought to involve an intramolecular PT from the carboxylic acid to another atom within the catalyst. The closest *meso* carbon is the most structurally and thermodynamically favorable proton acceptor site within the proton relay, forming the phlorin $[\mathbf{1}\text{-}\mathbf{H}_C]^{2-}$. As for [**3**], the phlorin stabilizes the ring conjugation due to ligand dearomatization in $[\mathbf{1}\text{-H}]^{2-}$. These properties of the hangman porphyrin have significant implications for the HER mechanism.

The H_2 evolution mechanism was explored for all of these Co porphyrins in weak- and strong-acid regimes, corresponding to experiments performed with benzoic and tosic acids. Under strong-acid conditions, [**1**-H], [**2**], and [**3**] all behave similarly and can evolve H_2 from a Co hydride intermediate. Under weak-acid conditions, [**1**-H] evolves hydrogen at a potential 100−200 mV less negative than that for [**2**] or [**3**].[24] The calculations were consistent with previous experiments indicating that the PCET step following the initial reduction of $[\mathbf{1}\text{-H}]^0$ to $[\mathbf{1}\text{-H}]^-$ occurs by a sequential ET-PT pathway. In this ET-PT pathway, the reduction of $[\mathbf{1}\text{-H}]^-$ to $[\mathbf{1}\text{-H}]^{2-}$ is followed by intramolecular PT. According to the calculations, the most thermodynamically and structurally favorable intramolecular PT reaction produces the dianonic phlorin $[\mathbf{1}\text{-}\mathbf{H}_C]^{2-}$, which differs from the previous proposal of a cobalt hydride intermediate.[25] The calculated free energy barrier and associated rate constant for the PT reaction from the carboxylic acid to the *meso* carbon (9.0 kcal/mol; $k_{PT} = 1.4 \times 10^6\ s^{-1}$) are consistent with the experimentally measured rate constant ($k_{PT} \approx 8.5 \times 10^6\ s^{-1}$). This agreement provides further support for an ET-PT mechanism that generates a phlorin intermediate rather than a metal hydride. Following the sequential ET-PT pathway, the dianionic phlorin $[\mathbf{1}\text{-}\mathbf{H}_C]^{2-}$ may be protonated at the carboxylate to form the doubly protonated species $[\mathbf{1}\text{-}\mathbf{HH}_C]^-$. This complex can be spontaneously reduced at the catalytic potential $E_{cat}[\mathbf{1}] \approx -1.9$ V vs Fc^+/Fc to $[\mathbf{1}\text{-}\mathbf{HH}_C]^{2-}$. Subsequent elimination of H_2 is thermodynamically favorable, yielding a deprotonated $[\mathbf{1}]^{2-}$, which can be protonated from benzoic acid to form $[\mathbf{1}\text{-H}]^-$.

Storing reducing equivalents by reductive dearomatization and carbon-centered protonation, as exemplified in the conversion of $[\mathbf{1}\text{-H}]^0$ to $[\mathbf{1}\text{-}\mathbf{H}_C]^{2-}$, is similar to known strategies for storing formal hydride equivalents in both biology and synthetic chemistry. NADH, the reduction currency in biology, is generated by $2e^-/1H^+$ delivery to NAD^+.[61,62] Reductive protonation of NAD^+ dearomatizes a pyridyl ring and stores reduction equivalents as a hydride on an sp^3 carbon center (Figure 7a). Hantzsch esters represent synthetic analogues of NADH and have been employed as H_2 surrogates in transfer hydrogenation reactions.[63] The reducing equivalents of Hantzsch esters can be generated by reductive dearomatiza-

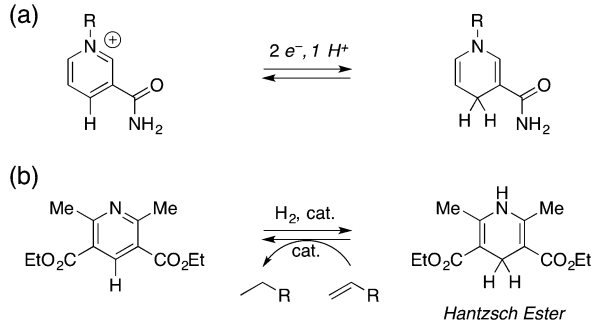

Figure 7. (a) Two-electron, one-proton reduction of NAD^+ generates NADH, in which a reducing equivalent is stored as a hydride at an sp^3 center (R = ADP-ribo). (b) Hantzsch esters are synthetic analogues of NADH and function as hydrogen surrogates in transfer hydrogenation.

dx.doi.org/10.1021/cs501454y | ACS Catal. 2014, 4, 4516−4526

tion of appropriately substituted pyridines (Figure 7b). Similar ligand-centered management of hydride equivalents have also been demonstrated in C-centered frustrated Lewis pair reactions for cleavage of H_2[64] and in dearomative M−L cooperation in Ru-pincer complexes.[65]

Thus, these calculations, supported by related examples from the literature, suggest that the HER mechanism of [**1**-**H**] could involve a phlorin intermediate under weak-acid conditions. This proposed mechanism will require testing and validation by further experimental studies aimed at identifying and characterizing a phlorin intermediate. Free-base phlorins are well-known, isolable compounds, which have been demonstrated to participate in multielectron redox chemistry.[66−70] Unique spectroscopic signatures of the phlorin complexes have been discovered and can be used in future experiments aimed at probing the proposed transient phlorin intermediate.[71] Furthermore, the analogous nickel hangman porphyrins, which have been proposed to follow a sequential PT-ET pathway,[59] may also evolve hydrogen through a phlorin intermediate.

■ ASSOCIATED CONTENT

Supporting Information

The following file is available free of charge on the ACS Publications website at DOI: 10.1021/cs501454y.

Discussion of computational benchmarking, calculation of H_2 production free energies, experimental methods, calculated relative free energies of structures optimized in the gas phase and solution, calculated bond distances and angles, calculated reduction potentials and relative pK_as, ^{1}H NMR and crystal structures of [**3**]$^-$, free energy diagrams of H_2 evolution catalyzed by [**3**] with tosic and benzoic acids, coordinates and energies of structures optimized in solution (PDF)

■ AUTHOR INFORMATION

Corresponding Author

*E-mail for S.H.-S.: shs3@illinois.edu.

Notes

The authors declare no competing financial interest.

■ ACKNOWLEDGMENTS

We are grateful to Thomas B. Rauchfuss, D. Kwabena Bediako, Mioy T. Huynh, Soumya Ghosh, and Alexander Soudackov for meaningful discussion and helpful advice. B.H.S. and S.H.-S. acknowledge support for the computational work by the Center for Chemical Innovation of the National Science Foundation (Solar Fuels, Grant No. CHE-1305124). The contributions by A.G.M., T.H., D.C.P., and D.G.N. are based on work supported by the U.S. Department of Energy Office of Science, Office of Basic Energy Sciences Energy Frontier Research Centers program under Award Number DE-SC0009758.

■ REFERENCES

(1) Lewis, N. S.; Nocera, D. G. *Proc. Natl. Acad. Sci. U.S.A.* **2006**, *103*, 15729−15735.
(2) Nocera, D. G. *Inorg. Chem.* **2009**, *48*, 10001−10017.
(3) Cukier, R. I.; Nocera, D. G. *Annu. Rev. Phys. Chem.* **1998**, *49*, 337−369.
(4) Mayer, J. M. *Annu. Rev. Phys. Chem.* **2004**, *55*, 363−390.
(5) Huynh, M. H. V.; Meyer, T. J. *Chem. Rev.* **2007**, *107*, 5004−5064.
(6) Hammes-Schiffer, S.; Soudackov, A. V. *J. Phys. Chem. B* **2008**, *112*, 14108−14123.
(7) Costentin, C. *Chem. Rev.* **2008**, *108*, 2145−2179.
(8) Costentin, C.; Robert, M.; Savéant, J.-M. *Chem. Rev.* **2010**, *110*, PR1−PR40.
(9) Hammes-Schiffer, S.; Stuchebrukhov, A. A. *Chem. Rev.* **2010**, *110*, 6939−6960.
(10) Wilson, A. D.; Shoemaker, R. K.; Miedaner, A.; Muckerman, J. T.; DuBois, D. L.; Rakowski DuBois, M. *Proc. Natl. Acad. Sci. U.S.A.* **2007**, *104*, 6951−6956.
(11) Barton, B. E.; Rauchfuss, T. B. *Inorg. Chem.* **2008**, *47*, 2261−2263.
(12) DuBois, D. L.; Bullock, R. M. *Eur. J. Inorg. Chem.* **2011**, 1017−1027.
(13) O'Hagen, M.; Shaw, W. J.; Raugei, S.; Chen, S.; Yang, J. Y.; Kilgore, U. J.; DuBois, D. L.; Bullock, R. M. *J. Am. Chem. Soc.* **2011**, *133*, 14301−14312.
(14) Horvath, S.; Fernandez, L. E.; Soudackov, A. V.; Hammes-Schiffer, S. *Proc. Natl. Acad. Sci. U.S.A.* **2012**, *109*, 15663−15668.
(15) Fernandez, L. E.; Horvath, S.; Hammes-Schiffer, S. *J. Phys. Chem. Lett.* **2013**, *4*, 542−546.
(16) Chen, S.; Ho, M.-H.; Bullock, R. M.; DuBois, D. L.; Dupuis, M.; Rousseau, R.; Raugei, S. *ACS Catal.* **2014**, *4*, 229−242.
(17) Le Goff, A.; Artero, V.; Jousselme, B.; Tran, P. D.; Guillet, N.; Métayé, R.; Fihri, A.; Palacin, S.; Fontecave, M. *Science* **2009**, *326*, 1384−1387.
(18) Dempsey, J. L.; Brunschwig, B. S.; Winkler, J. R.; Gray, H. B. *Acc. Chem. Res.* **2009**, *42*, 1995−2004.
(19) Liu, T.; Li, B.; Popescu, C. V.; Bilko, A.; Pérez, L. M.; Hall, M. B.; Darensbourg, M. Y. *Chem.—Eur. J.* **2010**, *16*, 3083−3089.
(20) McNamara, W. R.; Han, Z.; Alberin, P. J.; Brennessel, W. W.; Holland, P. L.; Eisenberg, R. *J. Am. Chem. Soc.* **2011**, *133*, 15368−15371.
(21) McNamara, W. R.; Han, Z.; Yin, C.-J.; Brennessel, W. W.; Holland, P. L.; Eisenberg, R. *Proc. Natl. Acad. Sci. U.S.A.* **2012**, *109*, 15594−15599.
(22) Valdez, C. N.; Dempsey, J. L.; Brunschwig, B. S.; Winkler, J. R.; Gray, H. B. *Proc. Natl. Acad. Sci. U.S.A.* **2012**, *109*, 15589−15593.
(23) Andreiadis, E. S.; Jacques, P.-A.; Tran, P. D.; Leyris, A.; Chavarot-Kerlidou, M.; Jousselme, B.; Matheron, M.; Pécaut, J.; Palacin, S.; Fontecave, M.; Artero, V. *Nat. Chem.* **2013**, *5*, 48−53.
(24) Lee, C. H.; Dogutan, D. K.; Nocera, D. G. *J. Am. Chem. Soc.* **2011**, *133*, 8775−8777.
(25) Roubelakis, M. M.; Bediako, D. K.; Dogutan, D. K.; Nocera, D. G. *Energy Environ. Sci.* **2012**, *5*, 7737−7740.
(26) Perdew, J. P. *Phys. Rev. B* **1986**, *33*, 8822−8824.
(27) Becke, A. D. *Phys. Rev. A* **1988**, *38*, 3098−3100.
(28) Becke, A. D. *J. Chem. Phys.* **1993**, *98*, 5648−5652.
(29) Lee, C.; Yang, W.; Parr, R. G. *Phys. Rev. B* **1988**, *37*, 785−789.
(30) Tao, J. M.; Perdew, J. P.; Staroverov, V. N.; Scuseria, G. E. *Phys. Rev. Lett.* **2003**, *91*, 146401.
(31) Zhao, Y.; Truhlar, D. G. *J. Chem. Phys.* **2006**, *125*, 194101.
(32) Grimme, S. *J. Comput. Chem.* **2006**, *27*, 1787−1799.
(33) Becke, A. D. *J. Chem. Phys.* **1997**, *107*, 8554−8560.
(34) Kamiya, M.; Tsunea, T.; Hirao, K. *J. Chem. Phys.* **2002**, *117*, 6010−6015.
(35) Chai, J.-D.; Head-Gordon, M. *Phys. Chem. Chem. Phys.* **2008**, *10*, 6615−6620.
(36) Hariharan, P. C.; Pople, J. A. *Theor. Chim. Acta* **1973**, *28*, 213−222.
(37) Hehre, W. J.; Ditchfield, R.; Pople, J. A. *J. Chem. Phys.* **1972**, *56*, 2257−2261.
(38) Francl, M. M.; Pietro, W. J.; Hehre, W. J.; Binkley, J. S.; Gordon, M. S.; DeFrees, D. J.; Pople, J. A. *J. Chem. Phys.* **1982**, *77*, 3654−3665.
(39) Clark, T.; Chandrasekhar, J.; Spitznagel, G. W.; Schleyer, P. v. R. *J. Comput. Chem.* **1983**, *4*, 294−301.
(40) Frisch, M. J.; Trucks, G. W.; Schlegel, H. B.; Scuseria, G. E.; Robb, M. A.; Cheeseman, J. R.; Scalmani, G.; Barone, V.; Mennucci, B.; Petersson, G. A.; Nakatsuji, H.; Caricato, M.; Li, X.; Hratchian, H.

P.; Izmaylov, A. F.; Bloino, J.; Zheng, G.; Sonnenberg, J. L.; Hada, M.; Ehara, M.; Toyota, K.; Fukuda, R.; Hasegawa, J.; Ishida, M.; Nakajima, T.; Honda, Y.; Kitao, O.; Nakai, H.; Vreven, T.; Montgomery, J. A., Jr.; Peralta, J. E.; Ogliaro, F.; Bearpark, M.; Heyd, J. J.; Brothers, E.; Kudin, K. N.; Staroverov, V. N.; Kobayashi, R.; Normand, J.; Raghavachari, K.; Rendell, A.; Burant, J. C.; Iyengar, S. S.; Tomasi, J.; Cossi, M.; Rega, N.; Millam, J. M.; Klene, M.; Knox, J. E.; Cross, J. B.; Bakken, V.; Adamo, C.; Jaramillo, J.; Gomperts, R.; Stratmann, R. E.; Yazyev, O.; Austin, A. J.; Cammi, R.; Pomelli, C.; Ochterski, J. W.; Martin, R. L.; Morokuma, K.; Zakrzewski, V. G.; Voth, G. A.; Salvador, P.; Dannenberg, J. J.; Dapprich, S.; Daniels, A. D.; Farkas, Ö.; Foresman, J. B.; Ortiz, J. V.; Cioslowski, J.; Fox, D. J. *Gaussian 09, Revision C.1*; Gaussian, Inc., Wallingford, CT, 2009.

(41) Barone, V.; Cossi, M. *J. Phys. Chem. A* **1998**, *102*, 1995−2001.

(42) Cossi, M.; Rega, N.; Scalmani, G.; Barone, V. *J. Comput. Chem.* **2003**, *24*, 669−681.

(43) Floris, F.; Tomasi, J. *J. Comput. Chem.* **1989**, *10*, 616−627.

(44) Floris, F. M.; Tomasi, J.; Ahuir, J. L. P. *J. Comput. Chem.* **1991**, *12*, 784−791.

(45) Pierotti, R. A. *Chem. Rev.* **1976**, *76*, 717−726.

(46) Solis, B. H.; Hammes-Schiffer, S. *Inorg. Chem.* **2011**, *50*, 11252−11262.

(47) Solis, B. H.; Hammes-Schiffer, S. *Inorg. Chem.* **2014**, *53*, 6427−6443.

(48) Hansch, C.; Leo, A.; Taft, R. W. *Chem. Rev.* **1991**, *91*, 165−195.

(49) Solis, B. H.; Hammes-Schiffer, S. *J. Am. Chem. Soc.* **2011**, *133*, 19036−19039.

(50) McGuire, R., Jr.; Dogutan, D. K.; Teets, T. S.; Suntivich, J.; Shao-Horn, Y.; Nocera, D. G. *Chem. Sci.* **2010**, *1*, 411−414.

(51) Roubelakis, M. M.; Nocera, D. G., unpublished results.

(52) Hu, X.; Brunschwig, B. S.; Peters, J. C. *J. Am. Chem. Soc.* **2007**, *129*, 8988−8998.

(53) Fourmond, V.; Jacques, P.-A.; Fontecave, M.; Artero, V. *Inorg. Chem.* **2010**, *49*, 10338−10347.

(54) Peng, C.; Schlegel, H. B. *Isr. J. Chem.* **1993**, *33*, 449−454.

(55) Peng, C.; Ayala, P. Y.; Schlegel, H. B.; Frisch, M. J. *J. Comput. Chem.* **1996**, *17*, 49−56.

(56) Whitlock, H. W.; Bower, B. K. *Tetrahedron Lett.* **1965**, *52*, 4827−4831.

(57) Kobayashi, H.; Hara, T.; Kaizu, Y. *Bull. Chem. Soc. Jpn.* **1972**, *45*, 2148−2155.

(58) Baran, J. D.; Grönbeck, H.; Hellman, A. *J. Am. Chem. Soc.* **2014**, *136*, 1320−1326.

(59) Bediako, D. K.; Solis, B. H.; Dogutan, D. K.; Roubelakis, M. M.; Maher, A. G.; Lee, C. H.; Chambers, M. B.; Hammes-Schiffer, S.; Nocera, D. G. *Proc. Natl. Acad. Sci. U.S.A.* **2014**, *111*, 15001−15006.

(60) Venkataraman, C.; Soudackov, A. V.; Hammes-Schiffer, S. *J. Phys. Chem. C* **2008**, *112*, 12386−12397.

(61) Belenky, P.; Bogan, K. L.; Brenner, C. *Trends Biochem. Sci.* **2007**, *32*, 12−19.

(62) Pollak, N.; Dölle, C.; Ziegler, M. *Biochem. J.* **2007**, *402*, 205−218.

(63) Zheng, C.; You, S.-L. *Chem. Soc. Rev.* **2012**, *41*, 2498−2518.

(64) Boone, M. P.; Stephan, D. W. *Chem. Eur. J.* **2014**, *20*, 3333−3341.

(65) Zhang, J.; Leitus, G.; Ben-David, Y.; Milstein, D. *J. Am. Chem. Soc.* **2005**, *127*, 10840−10841.

(66) O'Brien, A. Y.; McGann, J. P.; G. Richard Geier, I. *J. Org. Chem.* **2007**, *72*, 4084−4092.

(67) Flint, D. L.; Fowler, R. L.; LeSaulnier, T. D.; Long, A. C.; O'Brien, A. Y.; G. Richard Geier, I. *J. Org. Chem.* **2010**, *75*, 553−563.

(68) Pistner, A. J.; Yap, G. P. A.; Rosenthal, J. *J. Phys. Chem. C* **2012**, *116*, 16918−16924.

(69) Pistner, A. J.; Lutterman, D. A.; Ghidiu, M. J.; Ma, Y.-Z.; Rosenthal, J. *J. Am. Chem. Soc.* **2013**, *135*, 6601−6607.

(70) Bruce, A. M.; Weyburne, E. S.; Engle, J. T.; Ziegler, C. J.; G. Richard Geier, I. *J. Org. Chem.* **2014**, *79*, 5664−5672.

(71) Pistner, A. J.; Lutterman, D. A.; Ghidiu, M. J.; Walker, E.; Yap, G. P. A.; Rosenthal, J. *J. Phys. Chem. C* **2014**, *118*, 14124−14132.